Catalysis Today xxx (xxxx) xxx

Contents lists available at ScienceDirect

Catalysis Today

journal homepage: www.elsevier.com/locate/cattod

Removal of metoprolol by means of photo-oxidation processes

Osmín Avilés-García [a], Jaime Espino-Valencia [b], Arisbeht Mendoza-Zepeda [a], Kingsley Donkor [c], Sharon Brewer [c], Rubi Romero [a], Reyna Natividad [a,*]

[a] Chemical Engineering Lab., Centro Conjunto de Investigación en Química Sustentable, UAEM-UNAM, Universidad Autónoma del Estado de México, km 14.5 Toluca-Atlacomulco Road, San Cayetano, Piedras Blancas, 50200 Toluca, Estado de México, Mexico
[b] Facultad de Ingeniería Química, Universidad Michoacana de San Nicolás de Hidalgo, Edif. V1, Ciudad Universitaria, 58060, Morelia, Michoacán, Mexico
[c] Department of Physical Sciences (Chemistry), Faculty of Science, Thompson Rivers University, 805 TRU Way, Kamloops, British Columbia V2C 0C8, Canada

ARTICLE INFO

Keywords:
β-blocker
Doped TiO_2
Photocatalysis
Photo-Fenton-like
Photo-Fenton

ABSTRACT

In this study, β-blocker metoprolol was degraded by photocatalysis and photo-Fenton catalyzed by doped TiO_2. The effect of two main variables was elucidated, content and type of doping cation (Fe or Cu). The catalysts were synthesized by Evaporation-Induced Self-Assembly (EISA) method and their performance was compared with typical Degussa P25. All synthesized materials were found to be mesoporous with a specific surface in the range of 121–242 m^2/g, they all exhibited anatase phase, and crystallites in the range of 6–10 nm. The use of X-ray photoelectron spectroscopy (XPS) allowed to establish not only the presence of the expected Ti^{4+} but also Ti^{3+} species. Cu^{2+} and Fe^{3+} species were also identified in the doped catalysts. It was found that the addition of Cu and Fe diminished the energy band gap of synthesized TiO_2, from 3.20 eV to 2.58 and 2.64, respectively. The content of Cu is directly correlated with this effect. In photocatalysis, the doping of TiO_2 did not have an effect of metoprolol degradation rate. This was improved, however, approximately 60% by the synthesized TiO_2 compared to Degussa P25. On the other hand, the photo-Fenton-like process catalyzed by Cu-TiO_2 exhibited the highest degradation (total removal) and mineralization extent (90%), being faster than the photocatalytic process and the UV-H_2O_2 system. Another difference between both methods, was the amount and type of intermediates generated. These were identified by LC-MS. Photo-Fenton catalyzed by Cu/TiO_2 can be considered as an effective process with high oxidative power in the metoprolol degradation.

1. Introduction

A large number of pharmaceutical products are consumed worldwide, as a result, these have been found in wastewater from hospitals, homes and pharmaceutical industries [1]. The amount of these drugs in the effluents varies from less than 1 mg/L to 100 mg/L, which generates a great impact on the environment because they exhibit biological activity and recalcitrant nature [2]. The removal of this type of compounds in treatment plants by conventional methods is not completely achieved, being found at low concentrations in drinking and surface water. In this context, β-blockers are a highly consumed class of pharmaceutical products used for the treatment of diseases in the cardiovascular system and they are considered emerging pollutants [3]. Although the main source of β-blockers to the environment is due to discharges from the pharmaceutical industry, it is considered that approximately 5% of oral administration in patients with cardiovascular problems is excreted without any change to the waste sources. Among the β-blockers, one of the most used is metoprolol (MET) which has been detected and quantified in wastewater effluents [4]. Therefore, its elimination is an important issue because of the risks it generates [5] as an emerging pharmaceutical pollutant.

The removal of metoprolol has already been studied through different AOPs, such as UV (monochromatic radiation) [6], ozone (O_3), O_3/UV, O_3/hydrogen peroxide (H_2O_2) [7], UV/H_2O_2 [8], heterogeneous photocatalysis [9], Fenton and photo-Fenton [10], achieving more than 70% removal in terms of mineralization through photo-induced processes. Specifically speaking, regarding photocatalysis and photo-Fenton, the comparison of the results attained and reported by the aforesaid documents is not straightforward since they have been performed in different reactors. Thus, the objective of this work was to compare the degradation and mineralization of metoprolol by using TiO_2 doped with different atomic percentages of iron (Fe) or copper (Cu) cations by photocatalysis, and by photo-Fenton-like, i.e. adding H_2O_2 to the process. The catalysts were synthesized by Evaporation-Induced

* Corresponding author.
E-mail address: rnatividadr@uaemex.mx (R. Natividad).

https://doi.org/10.1016/j.cattod.2021.06.014
Received 11 March 2021; Received in revised form 27 May 2021; Accepted 16 June 2021
Available online 26 June 2021

Self-Assembly (EISA) method and characterized by several techniques. Additionally, the produced intermediates were identified during the processes of MET degradation and a pathway for each process was proposed.

Photocatalysis using titanium dioxide (TiO_2) as a semiconductor has been widely used for environmental applications in both water and air [11]. TiO_2 is considered a good photocatalyst due to its high efficiency and stability, as well as low cost and toxicity [12]. However, this has some disadvantages associated with the high recombination rate and low transfer of photogenerated charges (e^-_{cb}/h^+_{vb}) [13]. To avoid these drawbacks, some metallic species can be incorporated into TiO_2 matrix by doping. The addition of cations, such as iron or copper, has shown improved photocatalytic activity of titania in aqueous media [14,15]. In addition, when hydrogen peroxide (H_2O_2) is present as an external oxidant, in combination with UV radiation and TiO_2 doped with iron, the process is called Photo-Fenton because the metals carry out electronic transfers that allow, together with the H_2O_2, the generation of more hydroxyl radicals [16]. In both cases, either by photocatalysis and photo-Fenton, it is of special interest to study the effect of the doping cation and also to be able to compare them with the photolytic processes for this purpose (UV, UV/H_2O_2) [17,18], which could efficiently affect the oxidation efficiency and obtained products. In this sense, it has been reported in photo-Fenton processes [19], that the presence of copper in the catalyst improves its photocatalytic efficiency.

2. Experimental

2.1. Chemicals

Titanium (IV) butoxide [$Ti(OC_4H_9)_4$, 97%], copper (II) nitrate trihydrate [$Cu(NO_3)_2 \cdot 3H_2O$, 99%] and iron (III) nitrate nanohydrate [$Fe(NO_3)_3 \cdot 9H_2O$, 99%], were used as precursors of Ti, Cu and Fe species, respectively. Ethyl alcohol (C_2H_6O, 99.5%), P123 copolymer ($EO_{20}PO_{70}EO_{20}$) and nitric acid (HNO_3, 70%) were used as solvent, surfactant and catalyst, respectively. Metoprolol tartrate salt (MET) [$(C_{15}H_{25}NO_3)_2 \cdot C_4H_6O_6$, >98%] was used as the pharmaceutical compound for photodegradation tests. All aforementioned reagents were analytical grade and were supplied by Sigma-Aldrich. Acetonitrile (CH_3CN, HPLC grade) and formic acid (HCOOH) were used to prepare the organic phase in the LC/MS analysis. Hydrogen peroxide (H_2O_2, 30% w/w) was used without further purification. Deionized water (Barnstead Easypure RoDi, Thermo Scientific) was used during all experiments.

2.2. Synthesis of catalysts

The following molar composition of reagents was used to synthesize the materials through EISA method: 5.8×10^{-3} titanium butoxide: 1.085×10^{-1} ethanol: 1.03×10^{-4} surfactant: 2.06×10^{-2} nitric acid. The synthesis was carried out as follows: a solution was prepared with the Ti precursor and the solvent, and then the P123 surfactant was incorporated. The precursors of doping species were subsequently added in atomic percentages M/(M + Ti) = 1, 3 and 5, where M represents Cu or Fe. Finally, the acid was added by dripping. The resulting mixture was kept under vigorous stirring for 3 h and dried in a rotary evaporator. The solid obtained was heat treated at 400 °C at a slow heating rate (1 °C min^{-1}). Pure titania was also synthesized through the aforementioned methodology, but without incorporating copper or iron species. Commercial photocatalyst (TiO_2 P25, Degussa) was also tested for comparison purposes.

2.3. Characterization of catalysts

The structural properties of all prepared materials were determined by X-ray diffraction (XRD) in a D8 Advance diffractometer (Bruker) using Cu Kα radiation source at 1.54 Å. XRD patterns were analyzed from 22° to 66° in 2θ range with steps of 0.0205° per second, at 25 mA and 30 kV. Additionally, the crystallite sizes were estimated according to the Scherrer equation ($d = 0.9\lambda/\beta \cos\theta$; where λ is the wavelength; β is the full width at half maximum value of XRD peak; and θ is the Bragg's angle).

Specific surface areas were determined by BET method and average pore diameters by BJH method of the synthesized catalysts in an Autosorb iQ analyzer (Quantachrome) through N_2 adsorption–desorption isotherms at 77 K (liquid nitrogen temperature). The catalysts were vacuum-degassed before analysis at 200 °C for 2 h.

Transmission electron microscopy (TEM, JEOL 2200Fs+Cs) was used to observe the crystalline particles and the elemental composition of the materials was analyzed with a detector of energy dispersive X-ray spectroscopy (EDS) OXFORD INCA under the following conditions: high voltage of 200 kV and magnifications to scale of approximately 1 μm at 20 kx.

Diffuse reflectance by UV–vis absorption was applied in all solids to estimate their band gap energies with a Lambda 35 spectrophotometer (Perkin-Elmer) by coupling a RSA-PE-20 integration sphere. The band gap energies were determined using the Kubelka-Munk function in order to obtain the adsorption spectra through the reflectance spectra.

Some synthesized materials were analyzed by X-ray photoelectron spectroscopy by using a JPS-9200 photoelectron spectrometer with an Al Kα source. The surface chemical analysis based on binding energies was corrected according to the reference energy of C 1 s at 284.6 eV.

2.4. Photodegradation tests

The degradation of metoprolol was evaluated by photocatalysis and photo-Fenton-like processes in a batch reactor with a total volume of 0.1 L. The initial metoprolol concentration was 50 mg/L, which corresponds to the actual concentration that may come from some industrial discharges [20]. The catalyst loading was 0.4 g L^{-1} [21,22] and was kept completely dispersed in the photo-reactor by continuous stirring. The source of radiation was a UV lamp placed inside the reactor with a monochromatic emission at 254 nm, a power of 8 W and an average radiation intensity of 166 W m^{-2}. The reactor was a glass cylinder (2.5 cm wide) and the lamp was placed at the center. The metoprolol solution was maintained at constant temperature (25 °C) by a thermal bath. The procedure of a typical experiment was as follows: batch reactor with metoprolol solution, followed by the addition of photocatalyst and finally turning on the radiation source (254 nm radiation from a lamp placed at the center of the reactor). For reactions that required hydrogen peroxide, this was incorporated in stoichiometric amount, according to the reaction of total MET mineralization, just before the lamp was turned on. All experiments were carried out at natural pH ($pH_0 \approx 5.6$).

2.5. Analytical methods

Aliquots were withdrawn from the reaction system at regular times, centrifuged to remove the solid and finally filtered using polyethersulfone membrane filters (0.45 μm pore size) prior to analysis. The identification of metoprolol and intermediates was carried out in a LC system (Agilent Series 1200) connected to a MS Q-TOF mass spectrometer (Agilent 6530) and equipped with an ESI source. The data were acquired in ESI+ mode between 30 and 500 *m/z* and the parameters used were: nebulizer, 13 psig; capillary, 3500 V; drying gas, 10 L min^{-1}; gas temperature, 350 °C; sheath gas temperature, 325 °C; sheath gas flow, 8 L min^{-1} and fragmentor, 60 V. The column, Eclipse plus-C18 (1.8 μm, 2.1 mm × 100 mm, Agilent), was kept at 35 °C with a flow rate (mobile phase) and an injection volume (sample volume) of 0.4 mL min^{-1} and 2 μL, respectively. The mobile phase had two components, aqueous phase (water) and organic phase (acetonitrile) both acidified with 1% v/v of formic acid. Additionally, an elution gradient referred to the organic phase (% acetonitrile) was used: 80% (0 min), 60% (3 min), 30% (5 min), 60% (5.3 min), 80% (5.5 min) and 80% (6 min).

The percentage of MET mineralization was determined in a TOC-

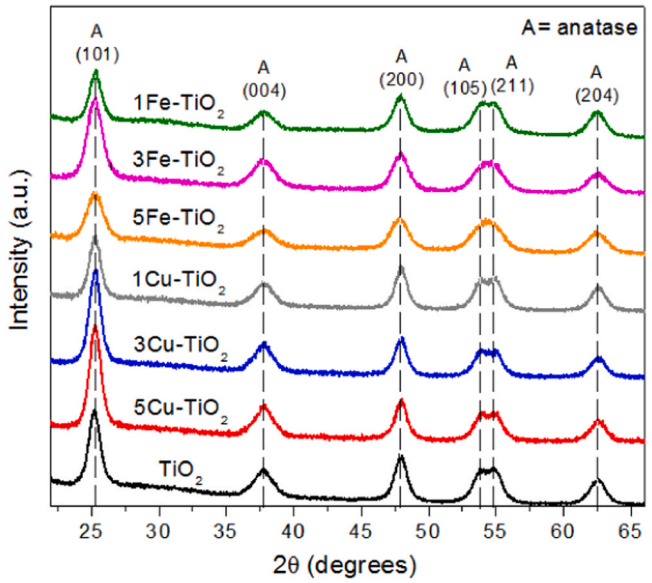

Fig. 1. X-ray diffraction patterns of undoped, Cu-doped and Fe-doped TiO_2 catalysts.

Table 1
Structural, textural and optical properties of the synthesized catalysts.

Catalyst	Anatase (101) plane	Average crystallite size (nm)	Specific surface area (m^2/g)	Average pore diameter (nm)	Pore volume (cm^3/g)	Band gap (eV)
1Fe-TiO_2	25.34	8.4	167	5.6	0.316	2.97
3Fe-TiO_2	25.30	6.1	176	4.9	0.303	2.79
5Fe-TiO_2	25.27	5.9	211	4.9	0.355	2.64
1Cu-TiO_2	25.30	8.8	202	6.6	0.424	3.16
3Cu-TiO_2	25.38	8.2	210	6.6	0.460	2.86
5Cu-TiO_2	25.25	7.9	242	5.6	0.481	2.58
TiO_2	25.21	8.2	121	5.6	0.262	3.20

VCSH analyzer (Mandel Scientific) by means of Total Organic Carbon (TOC). The analysis was carried out through the combustion catalytic oxidation at 680 °C of the previously acidified sample. In addition, it was pretreated with aeration to remove the inorganic carbon in order to determine the TOC content.

3. Results and discussion

3.1. Characterization

The X-ray diffraction patterns of the undoped TiO_2, Fe-doped and Cu-doped TiO_2 with different atomic amount of dopants are shown in Fig. 1. The diffraction peaks of all synthesized materials appeared at 25.2°, 37.8°, 47.9°, 53.8°, 54.8° and 62.6° at 2θ degrees, which correspond to the planes (101), (004), (200), (105), (211) and (204) of the anatase crystalline phase, respectively. No additional peaks attributed to the copper oxides (CuO, Cu_2O) or iron oxides (FeO, Fe_2O_3) were observed. This may be because the Cu or Fe species are very well distributed within the titania matrix or because their content is rather low and therefore could not be detected. The ionic radii of Cu^{2+} (0.072 nm) and Fe^{3+} (0.064 nm) are close to that of Ti^{4+} (0.068 nm). Thus, the difference in ion radii is less than 15% and according to Hume-Rothery's rules, the dopants are likely to be dissolved inside the anatase crystals [23]. The A (101) peak position presented in Table 1 exhibits a slight increase for all doped samples with respect to pure titania, which may be due to the distortion generated by the cations incorporated into the crystalline structure [24]. On the other hand, the crystallinity of TiO_2 was observed to increase with low percentages of dopant. The increase in atomic percentage reduced the crystallite size (see Table 1) and this can be ascribed to the generation of Cu-Ti-O and Fe-O-Ti bonds, which inhibits the growth rate of crystals [25]. The addition of dopants with oxidation states lower than Ti^{4+} generates anionic deficiencies due to oxygen vacancies, improving the separation of charges during photoactivity [26].

All prepared materials exhibited type IV isotherms and H2 hysteresis loops based on the IUPAC classification (see Fig. 2) [27], which indicates that the materials are of mesoporous structure with pores interconnected and homogeneously distributed in the solid particles. The surface areas were determined from the adsorption data in a relative pressure range of 0.05–0.3, and the pore diameters from the desorption data ($P/P_0 \geq 0.35$). As seen in Fig. 2, the increase of the adsorption bands at the saturation point for the doped samples, with respect to pure TiO_2, is related to larger surface areas. In addition, all catalysts presented only one pore size distribution according to Fig. 3. Specific

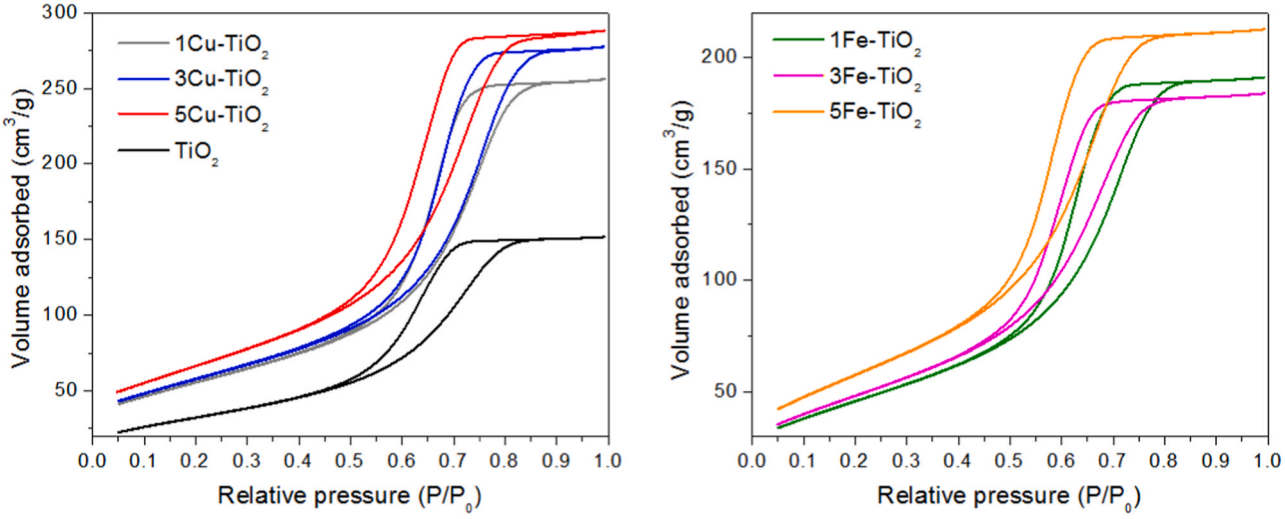

Fig. 2. N_2 adsorption-desorption isotherms of undoped, Cu-doped and Fe-doped TiO_2 materials.

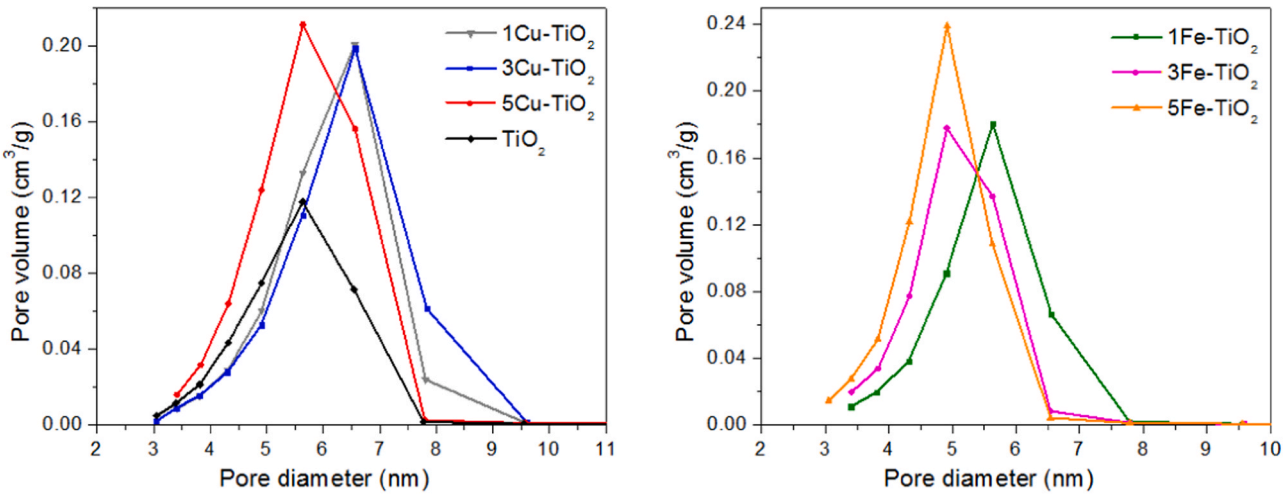

Fig. 3. Pore size distributions of undoped, Cu-doped and Fe-doped TiO_2 samples.

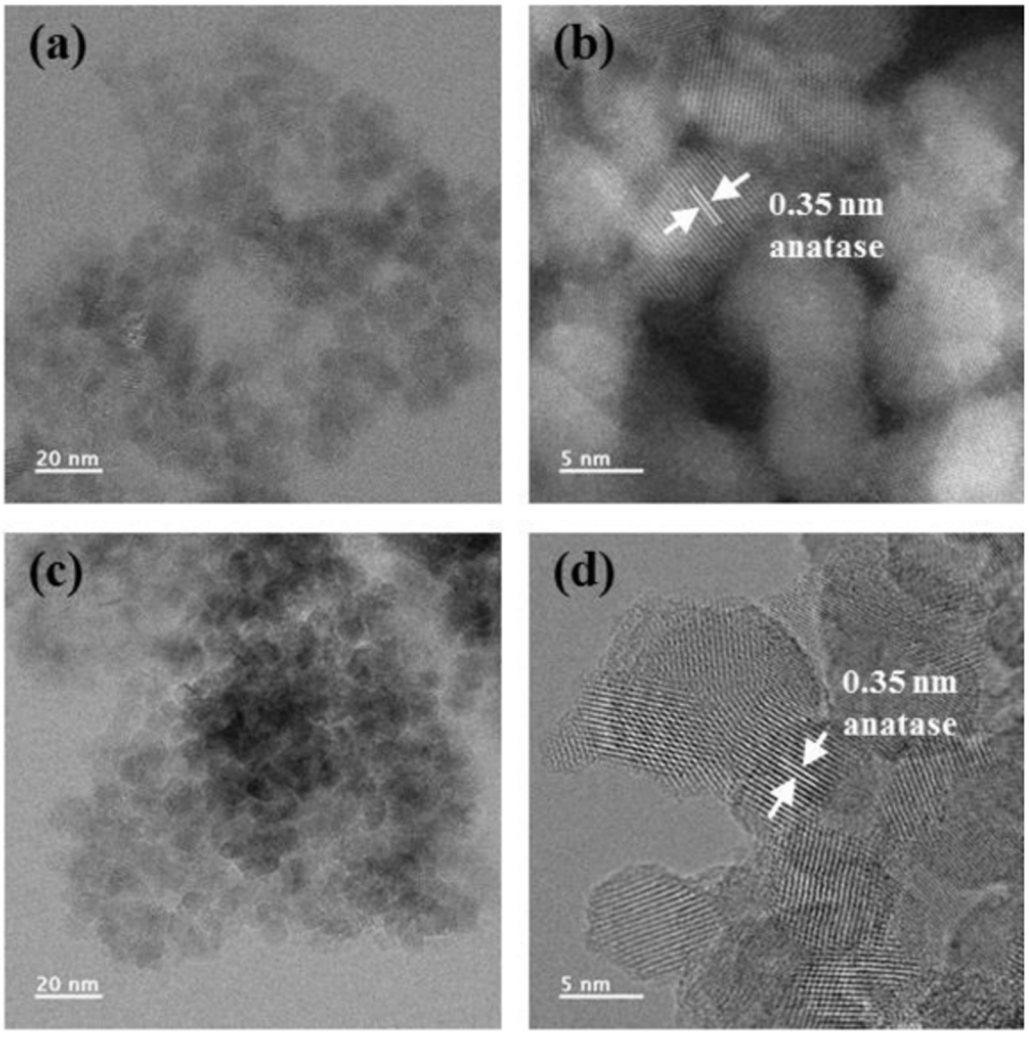

Fig. 4. TEM images and HRTEM images of samples (a, b) 1Cu-TiO_2 and (c, d) 1Fe-TiO_2.

surface areas, average pore diameters and total pore volumes are summarized in Table 1. The incorporation of Fe or Cu as dopant cations and their increase in atomic percentage increased the surface area of titania. This could be attributed to the decrease in crystallinity and the distribution of species into TiO_2. Cu-doped samples exhibited the best textural properties with surface areas of 242 $m^2\ g^{-1}$ compared to the undoped sample (121 $m^2\ g^{-1}$). Elevated surface areas may be beneficial for the adsorption of more organic molecules, thus achieving a higher removal rate [28,29].

The TiO_2 samples doped with 1 at% copper or iron, were analyzed by

Table 2
Elemental composition of the synthesized catalysts.

Sample	Analysis	Atomic percentages			
		Ti	O	Cu	Fe
	Theoretical	32.94	66.73	0.33	0.33
1Cu-TiO_2	EDS	27.81	71.90	0.29	–
1Fe-TiO_2	EDS	29.44	70.25	–	0.31

transmission electron microscopy and high-resolution transmission electron microscopy. Fig. 4(a, c) shows the TEM micrographs for both synthesized materials. Individual particles with crystallite sizes ranging from 6 to 10 nm can be observed, which is in accordance with the average crystallite size determined by the XRD analysis. The HRTEM micrographs presented in Fig. 4(c, d) exhibit well-defined lattice characteristics with high crystallinity. The distance between the parallel lines, with a value of 0.35 nm, corresponds to the interplanar distance *d* (101) of the anatase crystalline phase [30]. The EDS analysis are shown in Table 2 and Fig. 5, 0.29 at% Cu and 0.31 at% Fe could be detected, which match the theoretical value of dopants during synthesis.

The band gap energies of all synthesized materials were estimated by diffuse reflectance spectroscopy and their values are shown in Table 1. Fig. 6 shows the Tauc plots from the Kubelka-Munk function. These values correspond to the energy required to excite an electron in the semiconductor from its valence band to its conduction band, generating in this way electron/hole pairs during the photocatalytic activity. The band gap for anatase TiO_2 corresponds to a value of 3.20 eV [31]. The incorporation and increase of copper or iron cations into the titania generated variations in the band gap energies. Samples doped with Cu ions at high percentages exhibited the greatest reduction, which is due to charge transfer between oxygen 2*p*-orbitals and copper 3*d*-orbitals [32]. TiO_2 doped with a low concentration of Fe ions showed a significant reduction, compared to that doped with Cu. In this case, interactions of the Fe d-orbitals and Ti 3D-orbitals are present [33]. The presence of doping cations creates new energy states inside the band gap just below the conduction band of anatase, so the electronic excitation will require a lower energy level [34].

The oxidation state of the chemical species on the surface of 1Cu-doped and 1Fe-doped TiO_2 samples is shown in Fig. 7. The Ti 2p XPS spectra show peaks at 458.1 eV and 463.9 eV ascribed to Ti $2p_{3/2}$ and Ti $2p_{1/2}$ for Ti^{4+} states. The peaks located at binding energies of 455.6 eV and 462.4 eV are assigned to Ti $2p_{3/2}$ and Ti $2p_{1/2}$ for Ti^{3+} states (Fig. 7a) [35]. The presence of Ti^{3+} species is due to the formation of oxygen vacancies to preserve electronic neutrality. Fig. 7b exhibits the XPS spectra of O1s. Three peaks could be observed after the deconvolution of the O 1s signal at approximately 527.4 eV, 529.4 eV and 531.6 eV, which correspond to the oxygen lattice in O—Cu, O—Ti, and surface oxygen in O—H, respectively [36]. The presence of surface oxygen (hydroxyl groups) is related to defects due to the formed oxygen vacancies. Moreover, OH groups are considered beneficial for the photocatalytic activity, since from them the hydroxyl radicals, which are responsible for the oxidation of the organic compounds, can be easily generated [37]. The Cu 2p XPS spectra shows two peaks located at 932.6 eV and 951.9 eV, which are attributed to the binding energies of Cu $2p_{3/2}$ and Cu $2p_{1/2}$ states, respectively (see Fig. 7c). These peaks are assigned to the Cu^{2+} species forming Ti—O—Cu bonds by substitution of Ti^{4+} ions into anatase lattice [38], which generated changes in the electronic distribution of the atoms present on the catalytic surface. Fig. 7d shows the XPS spectra of Fe 2p region. Two peaks at binding energies of 711.7 eV and 724.20 eV are observed, which are ascribed to Fe $2p_{3/2}$ and Fe $2p_{1/2}$, respectively [39]. These signals confirm the presence of Fe^{3+} species in the TiO_2 structure.

3.2. Photodegradation of metoprolol

3.2.1. Photocatalysis

The catalysts synthesized with low and high levels of doping, as well as pure TiO_2 through the synthesis method and Degussa P25 as a commercial photocatalyst, were tested in the photocatalytic degradation of

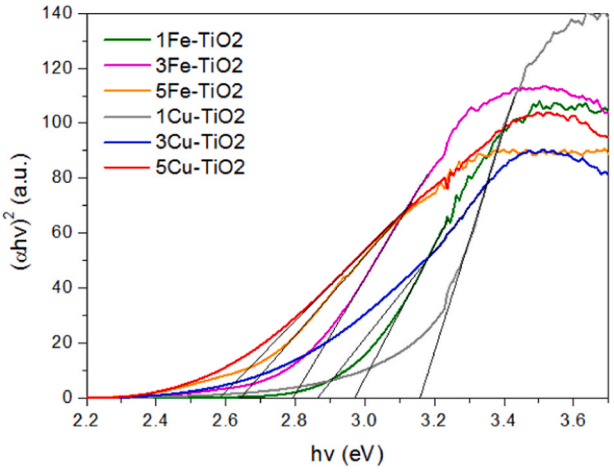

Fig. 6. Band gap energies (Tauc plots) of synthesized materials.

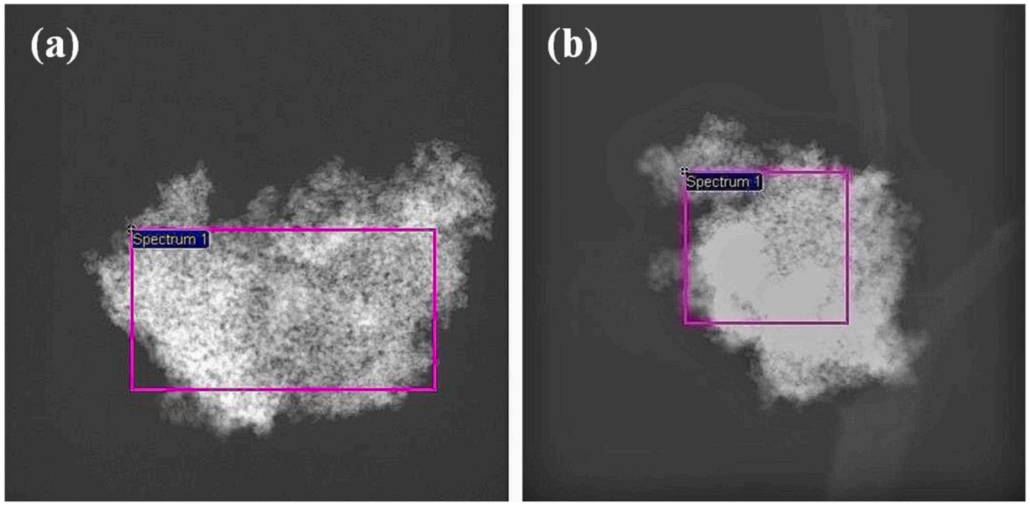

Fig. 5. EDS images of (a) 1Cu-TiO_2 and (b) 1Fe-TiO_2 samples.

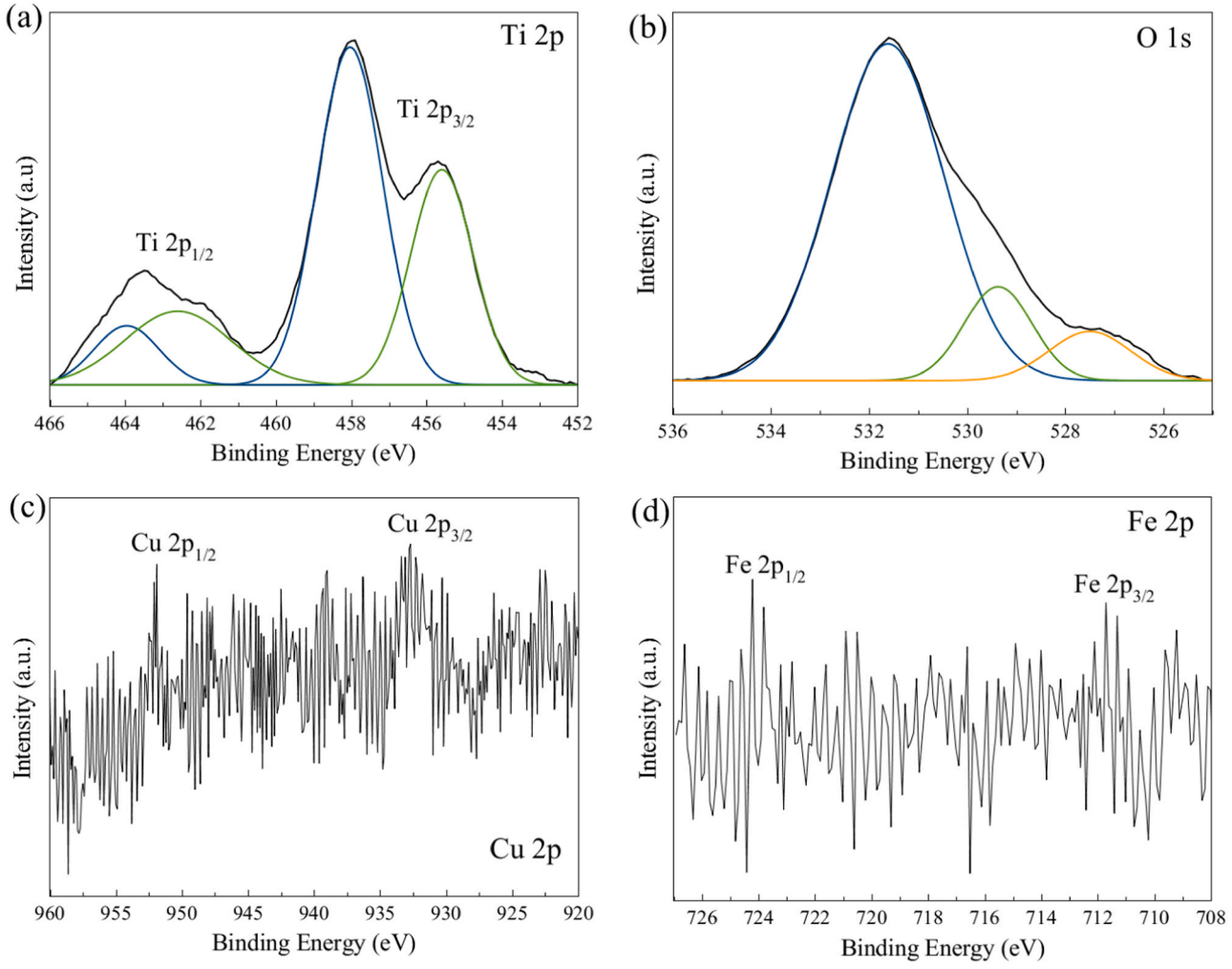

Fig. 7. XPS spectra of (a) Ti 2p, (b) O 1s, (c) Cu 2p of 1Cu-TiO_2 sample and (d) Fe 2p of 1Fe-TiO_2 sample.

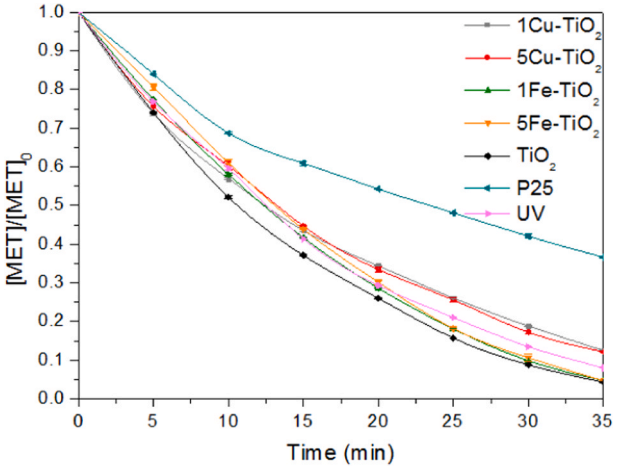

Fig. 8. Photocatalytic degradation of metoprolol over Cu-TiO_2, Fe-TiO_2, TiO_2 and P25, and removal by direct photolysis. $[MET]_0 = 18.70 \times 10^{-5}$ M, $C_{cat} = 4 \times 10^{-4}$ kg/L, $pH_0 = 5.6$ (natural), T = 298 K.

metoprolol (MET), as shown in Fig. 8. No significant effect of Cu or Fe content on MET degradation percentage was observed, since the samples doped with 1 and 5 at% Cu degraded approximately 88%, and those doped with 1 and 5 at% Fe degraded 95% after 35 min of irradiation. The presence of this type of dopant cations inside the titania did not enhance the percentage of MET photodegradation, because the non-dopant sample (TiO_2) achieved 95% degradation at the same time via hydroxyl radicals (Eqs. (1)–(4)). Direct photolysis of metoprolol has been previously reported [40,41] due to the absorption of radiation with

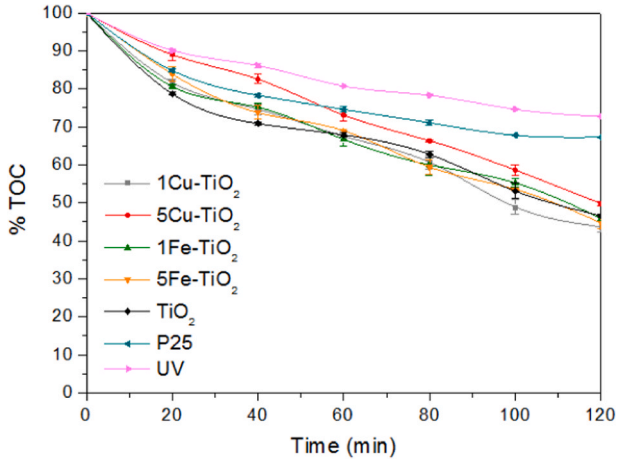

Fig. 9. Photocatalytic mineralization of metoprolol over Cu-TiO_2, Fe-TiO_2, TiO_2 and P25 catalysts, and direct photolysis. $[MET]_0 = 18.70 \times 10^{-5}$ M, $C_{cat} = 4 \times 10^{-4}$ kg/L, $pH_0 = 5.6$ (natural), T = 298 K.

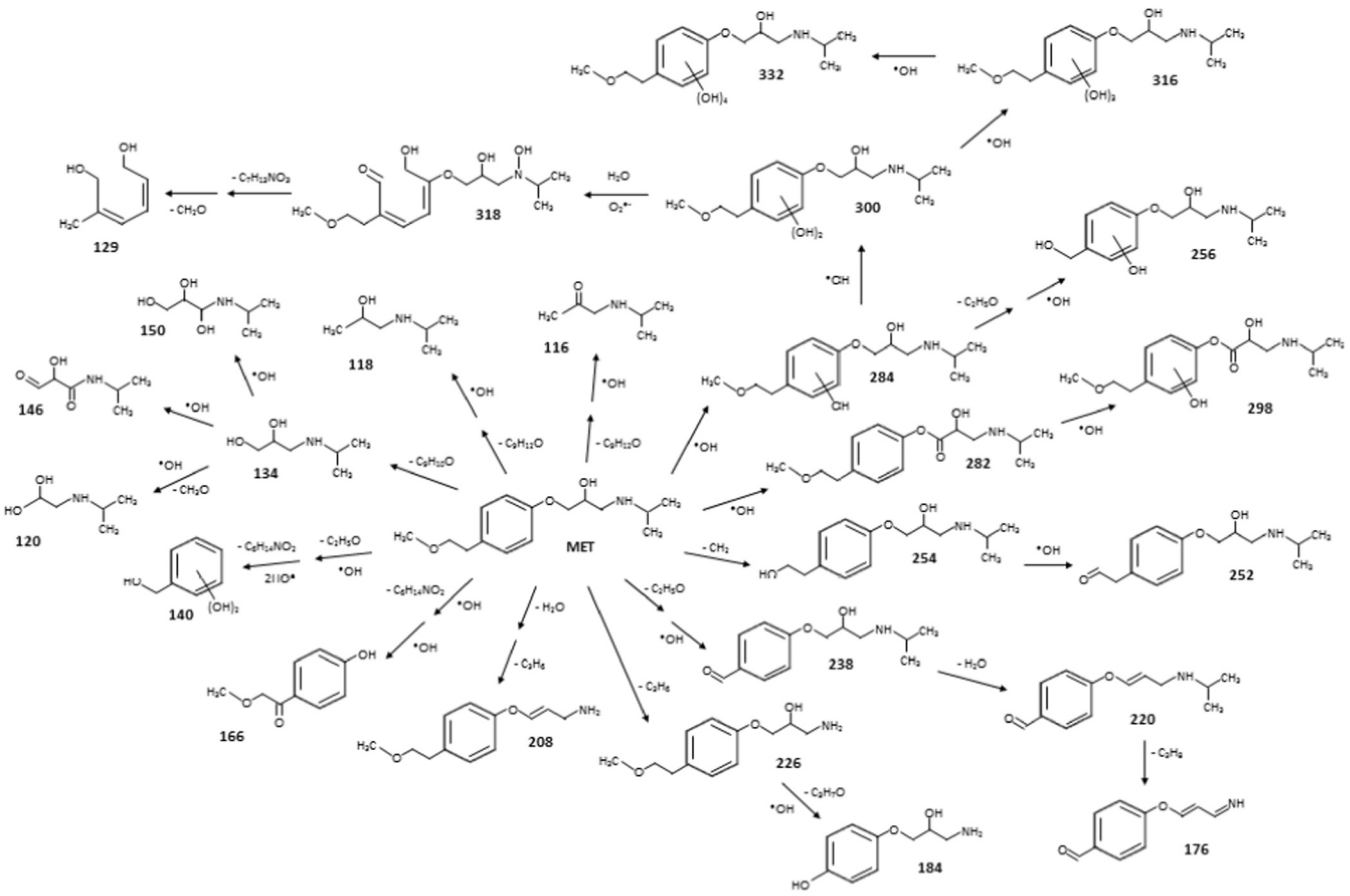

Fig. 10. Proposed pathways for the metoprolol photocatalytic degradation by Cu-TiO_2, Fe-TiO_2, TiO_2 and P25 catalysts.

enough energy (UVC) to degrade the organic compound (Eq. (5)) with a quantum yield of approximately 5×10^{-3} mol Einstein^{-1} [42]. Thus, from the results shown in Fig. 8, it can be concluded that MET degradation occurs mainly by Eq. (5) rather than by Eq. (4). This has been observed also with other molecules, acetaminophen for example [43]. Regarding Degussa P25, this might be causing a screening effect that prevents photons to reach metoprolol and therefore its oxidation rate is decreased and only 63% MET oxidation is achieved after 35 min of reaction.

$$TiO_2 + h\nu \rightarrow h^+_{vb} + e^-_{cb} \quad (1)$$

$$h^+_{vb} + {}^-OH \rightarrow {}^\bullet OH \quad (2)$$

$$h^+_{vb} + H_2O \rightarrow {}^\bullet OH + H^+ \quad (3)$$

$${}^\bullet OH + MET \rightarrow \text{intermediates} \rightarrow CO_2 + H_2O \quad (4)$$

$$MET + h\nu \rightarrow \text{intermediates} \quad (5)$$

At this point it was thought that the synthesized materials did not have photocatalytic activity. The mineralization results (Fig. 9), however, demonstrated otherwise. In this case, there is an important difference between the mineralization extent achieved by means of photolysis and that achieved with the prepared catalysts. In the first case, only 27% TOC removal was achieved while an approximately 55% TOC removal was achieved with the prepared materials after 120 min of treatment. This demonstrates the photocatalytic activity of the prepared materials towards the oxidation of the MET oxidation intermediates. The effect of the doping and content of dopant, however, is not appreciable since the use of pure TiO_2 and doped TiO_2 led to obtain around 55% of TOC removal after 120 min of treatment. The results shown in Fig. 9 are also evidence of the increased photoactivity exhibited by the prepared materials compared to the commercial photocatalyst, Degussa P25. This can be attributed to the Degussa P25 low surface area (50 m^2/g), non-porous structure and also different crystallinity. Degussa P25 is a mixture of Anatase and Rutile phases, while the synthesized materials do not show Rutile phase.

Several by-products of metoprolol oxidation were identified by LC/MS analysis during photocatalytic reactions based on the *m/z* (mass/charge) ratio (see Table S1). As can be seen, a total of 25 intermediates were present, except for $m/z = 128$, which was not identified in the photocatalysis with the materials 1Cu-TiO_2 and Degussa P25. Metoprolol ($C_{15}H_{25}NO_3$) was identified by its molecular weight at $m/z = 268$.

Fig. 10 shows a proposed photocatalytic degradation pathway of metoprolol and direct photolysis, with respect to the identified intermediates shown in Table S1. Intermediates *m/z* 284, 300, 316, 332 are formed by hydroxylation of the benzene ring from MET by $^\bullet$OH attack [44]. Intermediate *m/z* 256 is generated by $^\bullet$OH radical attack on the methoxyl side chain of *m/z* 284. The aromatic ring opening can take place due to hydroxylation followed by an attack to the amino group [45]. Intermediate *m/z* 129 can be formed because of reactions involving holes and $O_2^{\bullet-}$ radicals [46]. The attack of hydroxyl radicals on the C atom next to the ether group in the amine side chain of MET can form the intermediate *m/z* 282 [47]. Intermediate *m/z* 298 is produced by hydroxylation on the aromatic ring of *m/z* 282. Intermediates *m/z* 254, 252 and 238 can be generated by the elimination of the ether group in the methoxyl side chain, and the generation of an alcohol or aldehyde functional group by $^\bullet$OH radical attack [44]. The elimination of water from *m/z* 238 produces a carbonyl group and subsequently the formation of a double bond due to intramolecular electronic transfers, which can generate the intermediate *m/z* 220 [48]. Intermediate *m/z* 176 can be formed by the loss of isopropyl group from *m/z* 220. Oxidation on dimethylamine in the MET generates the intermediate *m/z* 226 [49].

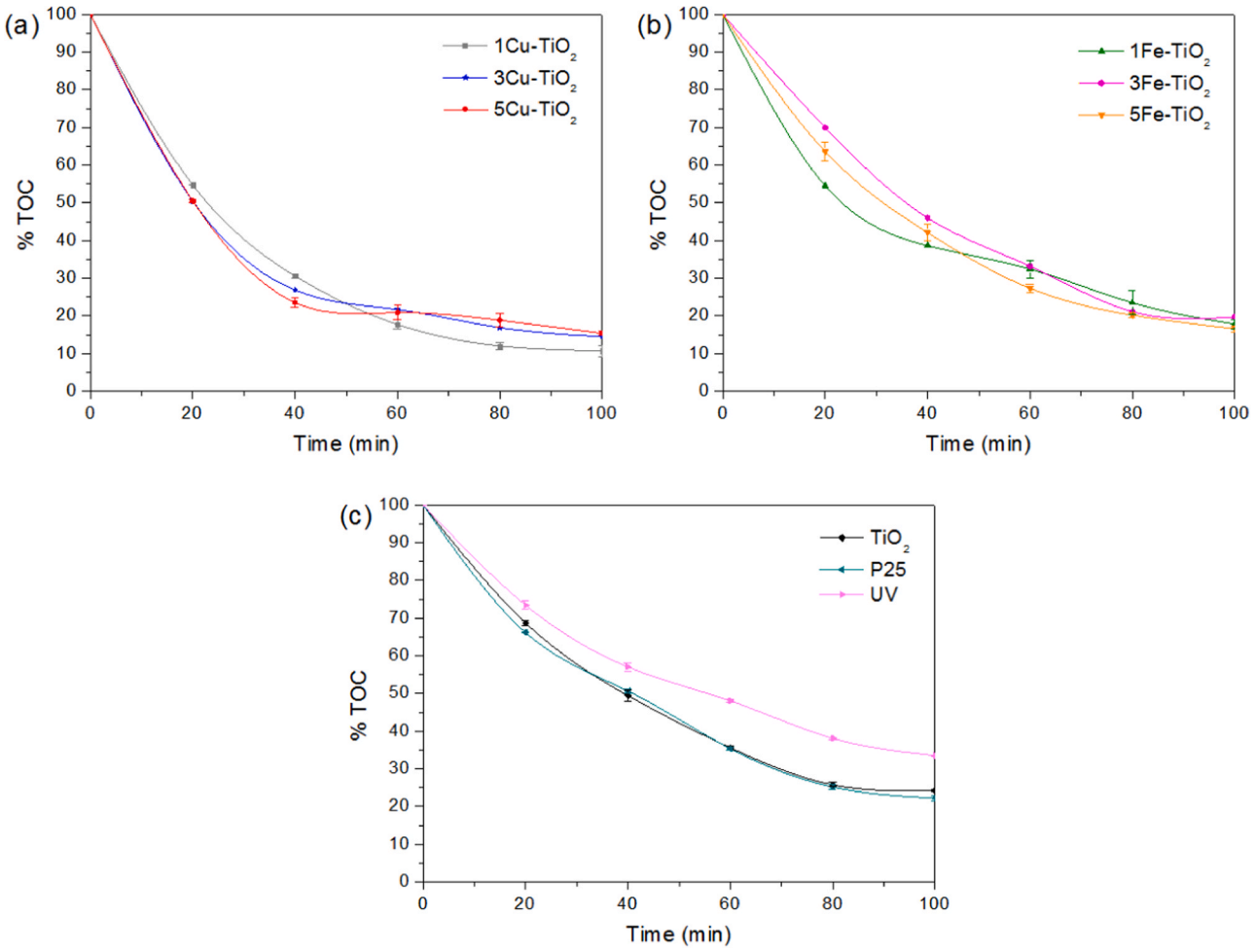

Fig. 11. Metoprolol mineralization profiles measured by TOC content over catalysts (a) Cu-TiO_2, (b) Fe-TiO_2, and (c) TiO_2, P25 and UV in combination with H_2O_2 at stoichiometric concentration. $[MET]_0 = 18.70 \times 10^{-5}$ M, $C_{cat} = 4 \times 10^{-4}$ kg/L, $pH_0 = 5.6$ (natural), T = 298 K.

Intermediate *m/z* 184 is produced by the attack of •OH radical on the ether side chain from *m/z* 226. The loss of the isopropyl group and water from the ethanolamine chain forms the intermediate *m/z* 208. Intermediate *m/z* 166 can be generated by MET hydroxylation with breaking of the amine lateral chain and a subsequent oxidation. Intermediate *m/z* 140 is produced by •OH attacks on both ether functional groups with alcohol formation from MET [50]. Intermediate *m/z* 118 is formed due to the loss of the benzene ring and the lateral chain by oxidation on the ether group. Intermediate *m/z* 134 is the dominant by-product in the degradation of metoprolol [51], which is generated by the breaking of the ether bond next to the aromatic ring in the aliphatic chain. Intermediates *m/z* 116, 120, 146 and 150 can be produced by the loss and oxidation of the hydroxyl group in the ethanolamine part [21]. In general, the degradation is based on the shortening of the side chain (methoxyl), hydroxylation of the aromatic ring and incorporation of hydroxyl radicals or cleavage in the amine side chain.

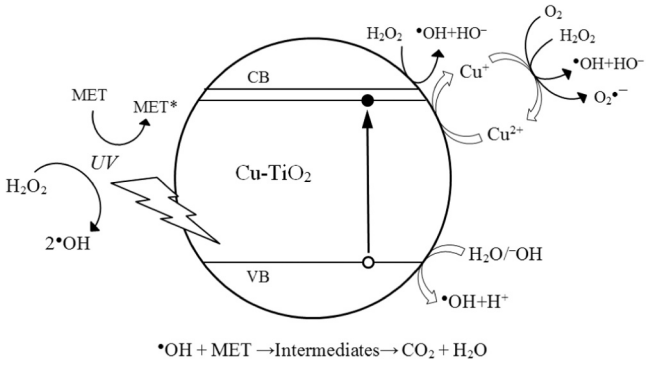

Fig. 12. Possible mechanism for metoprolol degradation by photo-Fenton-like over Cu-TiO_2 catalyst.

3.2.2. *Photo-Fenton-like process*

The hydrogen peroxide was incorporated in stoichiometric amount just before starting the irradiation. Fig. 11(a, b) shows the total organic carbon percentage temporary profiles during the photo-Fenton-like tests for all TiO_2 samples doped with Cu or Fe cations, respectively. As expected, the addition of H_2O_2 efficiently improves the MET mineralization, in comparison with photocatalysis (Fig. 9). As can be seen, in this case, the doping, either with Cu or Fe cations, exerts a positive effect mainly on mineralization rate. This effect is less pronounced on the maximum achieved mineralization extent. This being around 80% for most of the cases excepting for the copper doped TiO_2. In this case, the maximum TOC removal percentage is 90% with the lowest copper addition (Fig. 11a). This can be ascribed to copper being more active towards the dissociation of H_2O_2 (Eq. (13)) than iron, thus readily producing hydroxyl radicals. This can be due to their improved textural properties (see Table 1) and the fact that iron species can trap both electrons and holes, delaying the generation of active species [52]. Also, the redox potential of the TiO_2 conduction band is more negative than the potentials of the doping species Cu^{2+}/Cu^{+} and Fe^{3+}/Fe^{2+}, so electronic capture is favored [53,54]. Subsequently, the electrons can be

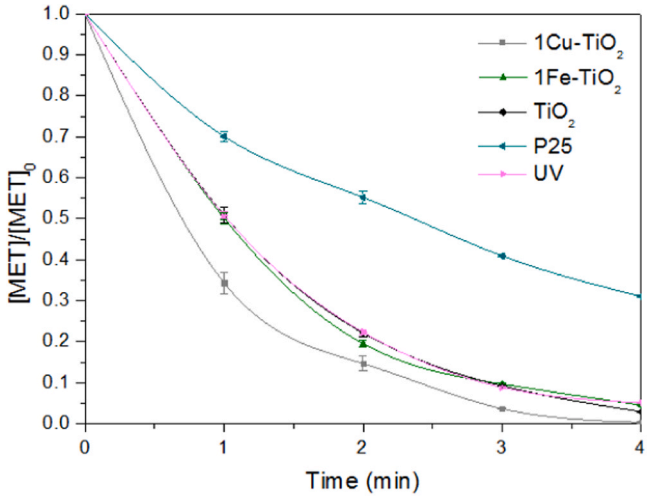

Fig. 13. Metoprolol degradation profiles over Cu-TiO_2, Fe-TiO_2, TiO_2, P25 catalysts and UV in combination with H_2O_2 stoichiometric. $[MET]_0 = 18.70 \times 10^{-5}$ M, $C_{cat} = 4 \times 10^{-4}$ kg/L, $pH_0 = 5.6$ (natural), T = 298 K.

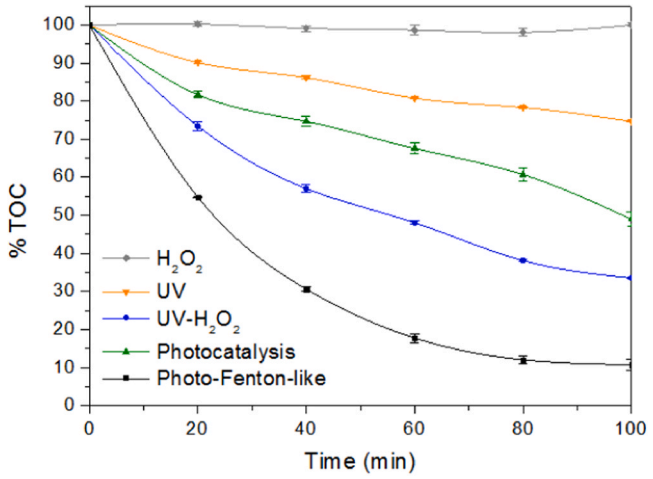

Fig. 15. Metoprolol mineralization profiles by the H_2O_2, UV, UV-H_2O_2, photocatalysis and photo-Fenton-like processes over Cu-doped TiO_2 catalyst. $[MET]_0 = 18.70 \times 10^{-5}$ M, $C_{cat} = 4 \times 10^{-4}$ kg/L, $pH_0 = 5.6$ (natural), T = 298 K.

scavenged by the oxygen present to generate other species, such as superoxide and hydroperoxyl radicals (Eqs. (8)–(10)) [55]. Dopant-free samples (TiO_2 and P25) show the lowest organic carbon reduction of 76% and 78%, respectively (see Fig. 11c). This might be because they do not contain doping species as electron traps, as well as their low surface areas. The hydrogen peroxide in combination with UVC radiation can generate hydroxyl radicals (Eq. (11)) [42]. In addition, H_2O_2 plays the role of external oxidant and generates through electron capture, $^{\bullet}OH$ radicals (Eq. (12)), which are the main species involved in the degradation of organic compounds (see Fig. 12) [56]. Fig. 11c shows the TOC reduction profile for the UV-H_2O_2 process, which achieved 66% after 100 min of irradiation.

$$Cu\text{-}TiO_2 + hv \rightarrow h^+_{vb} + e^-_{cb} \quad (6)$$

$$Cu^{2+} + e^-_{cb} \rightarrow Cu^+ \quad (7)$$

$$Cu^+ + O_2 \rightarrow Cu^{2+} + O_2^{\bullet -} \quad (8)$$

$$O_2^{\bullet -} + H^+ \rightarrow HO_2^{\bullet} \quad (9)$$

$$HO_2^{\bullet} \rightarrow H_2O_2 + O_2 \quad (10)$$

$$H_2O_2 + hv \rightarrow 2^{\bullet}OH \quad (11)$$

$$H_2O_2 + e^-_{cb} \rightarrow {}^{\bullet}OH + {}^{-}OH \quad (12)$$

$$Cu^+ + H_2O_2 \rightarrow Cu^{2+} + {}^{\bullet}OH + {}^{-}OH \quad (13)$$

The metoprolol degradation profiles are shown in Fig. 13. As can be seen, the material synthesized with low concentration of Fe, pure TiO_2 and the UV-H_2O_2 process show similar degradation profiles. The

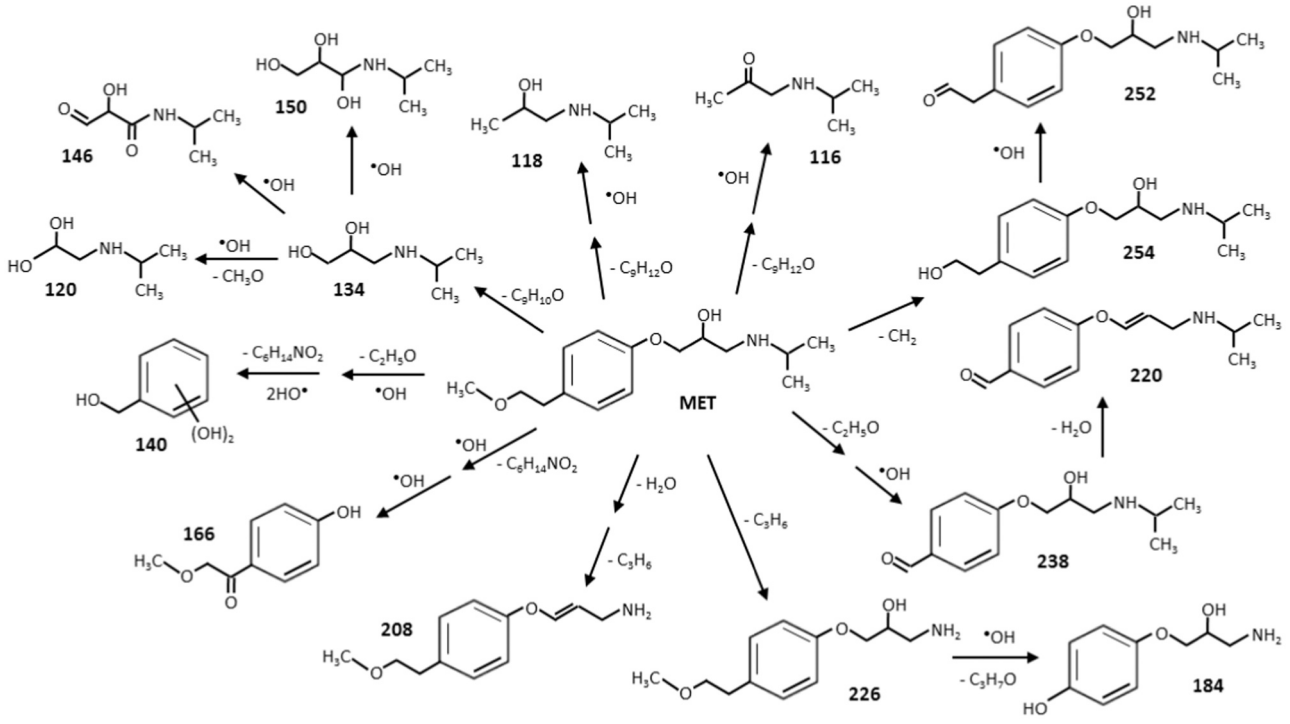

Fig. 14. Proposed pathways for the metoprolol degradation by photo-Fenton-like over Cu-TiO_2 and Fe-TiO_2 catalysts.

Table 3
Effect of the photo-oxidation process on metoprolol degradation and mineralization percentage, and on initial metoprolol degradation and mineralization rate.

Process	% MET degradation	% MET mineralization	Initial MET degradation rate × 10^7 (mol/g_{cat} s)	Initial MET mineralization rate × 10^3 (mg/g_{cat} s)	Reaction conditions	Catalyst	Ref.
UV	92 (35 min)	25 (100 min)	3.580	7.930	$[MET]_0$ = 50 mg/L	Cu-TiO_2	This work
UV-H_2O_2	91 (3 min)	66 (100 min)	48.02	22.65	H_2O_2 = stoich.		
Photocatalysis	87 (35 min)	51 (100 min)	4.850	16.24	pH_0 = 5.6		
Photo-Fenton-like	96 (3 min)	90 (100 min)	85.76	36.86	λ = 254 nm $V_{reaction}$ = 0.1 L		
Photo-Fenton	90 (60 min)	35 (300 min)	–	–	$[MET]_0$ = 50 mg/L H_2O_2 = excess pH_0 = – λ = 300–500 nm $V_{reaction}$ = 1 L	Fe^{2+}	[22]
Photo-Fenton	100 (3 min)	84 (150 min)	–	–	$[MET]_0$ = 50 mg/L H_2O_2 = excess pH_0 = 3 λ = 300–500 nm $V_{reaction}$ = 10 L	Fe^{2+}	[57]
Photocatalysis	90 (60 min)	80 (360 min)	–	–	$[MET]_0$ = 100 mg/L H_2O_2 = – pH_0 = 9.6 λ = 300–400 nm $V_{reaction}$ = 0.25 L	TiO_2	[9]
Photocatalysis	100 (180 min)	–	–	–	$[MET]_0$ = 20 mg/L H_2O_2 = excess pH_0 = 3 λ = 354 nm $V_{reaction}$ = 0.1 L	TiO_2/zeolite	[12]

commercial catalyst P25 exhibits the lowest degradation of metoprolol, 69% in 4 min. On the other hand, the 1Cu-TiO_2 sample shows the fastest degradation with more than 96% in 3 min of irradiation. Table S2 presents the intermediates formed during the photo-Fenton-like and UV-H_2O_2 processes. Intermediates *m/z* 129 and 176 were not identified during any test and intermediates *m/z* 282, 284 and 300 were not produced with the pure TiO_2 catalyst and the UV-H_2O_2 system. Degussa P25 was the catalyst that showed more intermediates, with a total of 23 compounds. Intermediates with high molecular weight (*m/z* 256, 282, 284, 298, 300, 316, 318 and 332) were not identified with TiO_2 samples doped with Cu or Fe, since fewer by-products were produced due to high oxidation, which is related to several effects, such as high surface area, appropriate concentration of electron acceptor doping species that reduce the recombination rate of photogenerated charges, and a greater amount of generated hydroxyl radicals. Fig. 14 shows proposed pathways for the metoprolol degradation by photo-Fenton-like over Cu-TiO_2 and Fe-TiO_2 catalysts, according to Table S2. At this point, it is worth pointing out that no MET removal in darkness was observed by the H_2O_2, catalyst and catalyst-H_2O_2 processes.

Fig. 15 shows the mineralization profiles of the main oxidation processes of metoprolol. As can be seen, the photolysis exhibits the lowest percentage of mineralization, followed by photocatalysis with a 51% reduction of TOC. Also, mineralization of metoprolol due only to the effect of H_2O_2 was observed to be negligible. Photo-Fenton-like process presents the highest mineralization of 90% with an initial rate of 36.83×10^{-3} mg/g_{cat}·s, faster than the UV-H_2O_2 system, as shown in Table 3. There are also shown in Table 3, the results reported in other works [9,12,22,57]. These results suggest a very competitive performance of the synthesized materials in terms of both, metoprolol and TOC removal.

It can be concluded that by performing the photo-Fenton like process with copper doped titania, a synergy between photocatalysis and photo-Fenton is obtained.

In addition, the complete removal of total organic carbon was not achieved at the end of all photo-degradation processes and this is mainly due to the presence of some intermediate recalcitrant compounds. 11 intermediaries were identified when metoprolol was oxidized by photolysis and photocatalysis, 4 intermediaries with the UV-H_2O_2 process and only 3 during the photo-Fenton-like process, as shown in Table 4. Some linear carboxylic acids (oxalic and oxamic) may also have been formed during metoprolol degradation [9], but they were not detected by LC-MS. If produced, these acids may come from the oxidation of intermediates *m/z* 116, 118, 120, 146 and 150 on the lateral part (ethanolamine side) of metoprolol, and they are the last species to mineralize directly to CO_2 [58]. It is worth pointing out that all the remaining by-products are not more toxic than the initial β-blocker, which has been reported by previous works during metoprolol degradation [57,59], thus achieving overall toxicity reduction.

Finally, it is worth pointing out that now that the catalytic activity of the synthesized materials was proven with UV irradiation and because of

Table 4
Intermediates identified at the end of each oxidation process.

m/z (+)	Elemental composition	Intermediates after photo-oxidation			
		UV	UV-H_2O_2	Photocatalysis	Photo-Fenton-like
116	$C_6H_{13}NO$	✓	–	✓	–
118	$C_6H_{15}NO$	✓	–	✓	–
120	$C_5H_{13}NO_2$	✓	–	✓	–
129	$C_7H_{12}O_2$	✓	–	–	–
134	$C_6H_{15}NO_2$	✓	–	✓	–
140	$C_7H_8O_3$	✓	✓	–	✓
146	$C_6H_{11}NO_3$	–	–	✓	–
150	$C_6H_{15}NO_3$	✓	–	✓	–
166	$C_9H_{10}O_3$	✓	–	✓	–
176	$C_{10}H_9NO_2$	✓	–	✓	–
184	$C_9H_{14}NO_3$	✓	✓	✓	✓
208	$C_{12}H_{17}NO_2$	–	–	✓	–
220	$C_{13}H_{17}NO_2$	✓	–	✓	–
226	$C_{12}H_{19}NO_3$	–	✓	–	✓
252	$C_{14}H_{21}NO_3$	–	✓	–	–

the calculated band gap energies, a next step on the application of these materials and in the light of sustainability, would be testing them with a lamp with a broader range of wavelengths.

4. Conclusions

Cu-TiO_2, Fe-TiO_2 and TiO_2 catalysts were synthesized by EISA method. This method allows to improve the textural properties of TiO_2 and the incorporation of Cu^{2+} and Fe^{3+} ions into the TiO_2 lattice. The presence of both cations modifies the textural and optical characteristics of pure TiO_2. Specific surface area increases, and energy band gap decreases with the cation content (2.58 eV for the 5 at% Cu-TiO_2).

The synthesized materials exhibited activity in the photocatalyzed mineralization of metoprolol degradation by-products. A 51% metoprolol mineralization is obtained by photocatalysis with the synthesized catalysts while only 30% and 25% is achieved with photocatalysis with TiO_2 Degussa P25 and photolysis, respectively. In the studied range, the incorporation of metal cations did not improve the rate nor the extent of metoprolol mineralization. The remained TOC is due to twenty-five intermediates detected during all photocatalytic tests and a pathway was proposed. This involved the attack of hydroxyl radicals on the side chains or by hydroxylation of the aromatic ring.

The metoprolol removal is about ten times faster with the photo-Fenton like process than with the photocatalytic or photolytic processes. Under photo-Fenton treatment, the incorporation of Cu^{2+} not only improves the metoprolol removal rate but also its mineralization rate and extent (90%). The recalcitrant compounds under this treatment were reduced to only 15, which were identified.

Finally, it can be concluded that 1 at% Cu-TiO_2 is an efficient catalyst to mineralize metoprolol under photo-Fenton treatment.

Declaration of Competing Interest

The authors declare that they have no known competing financial interests or personal relationships that could have appeared to influence the work reported in this paper.

Acknowledgements

Authors are grateful to PROMEP–Mexico (financial support through project 103.5/13/S257) and CONACYT–Mexico (project 269093). Osmín Avilés-García thanks COMECYT–Mexico for the financial support through CAT2021–0032. Authors are grateful to CCIQS from UAEM-UNAM and CIMAV-Mexico for the granted support. The technical support of Citlalit Martínez, Carlos Elías Ornelas Gutiérrez and Trent Hammer is also acknowledged.

Appendix A. Supporting information

Supplementary data associated with this article can be found in the online version at doi:10.1016/j.cattod.2021.06.014.

References

[1] L. Paredes, S. Murgolo, H. Dzinun, M.H. Dzarfan Othman, A.F. Ismail, M. Carballa, G. Mascolo, Application of immobilized TiO_2 on PVDF dual layer hollow fibre membrane to improve the photocatalytic removal of pharmaceuticals in different water matrices, Appl. Catal. B: Environ. 240 (2019) 9–18.

[2] A. Majumder, B. Gupta, A.K. Gupta, Pharmaceutically active compounds in aqueous environment: a status, toxicity and insights of remediation, Environ. Res. 176 (2019), 108542.

[3] S.J. Armaković, M. Grujić-Brojčin, M. Šćepanović, S. Armaković, A. Golubović, B. Babić, B.F. Abramović, Efficiency of La-doped TiO_2 calcined at different temperatures in photocatalytic degradation of β-blockers, Arab. J. Chem. 12 (2019) 5355–5369.

[4] N.H. Tran, M. Reinhard, K.Y.-H. Gin, Occurrence and fate of emerging contaminants in municipal wastewater treatment plants from different geographical regions-a review, Water Res. 133 (2018) 182–207.

[5] H. Martínez-Rodríguez, K. Donkor, S. Brewer, M. Galar-Martínez, N. SanJuan-Reyes, H. Islas-Flores, L. Sánchez-Aceves, A. Elizalde-Velázquez, L.M. Gómez-Oliván, Metoprolol induces oxidative damage in common carp (Cyprinus carpio), Aquat. Toxicol. 197 (2018) 122–135.

[6] L. Zhan, W. Li, L. Liu, T. Han, M. Li, Z. Qiang, Degradation of micropolluants in flow-through VUV/UV/H_2O_2 reactors: effects of H_2O_2 dosage and reactor internal diameter, J. Environ. Sci. (2021).

[7] D. Krakkó, Á. Illés, V. Licul-Kucera, B. Dávid, P. Dobosy, A. Pogonyi, A. Demeter, V. G. Mihucz, S. Dóbé, G. Záray, Application of (V)UV/O_3 technology for post-treatment of biologically treated wastewater: a pilot-scale study, Chemosphere 275 (2021), 130080.

[8] M.H.F. Graumans, W.F.L.M. Hoeben, M.F.P. van Dael, R.B.M. Anzion, F.G. M. Russel, P.T.J. Scheepers, Thermal plasma activation and UV/H_2O_2 oxidative degradation of pharmaceutical residues, Environ. Res. 195 (2021), 110884.

[9] E. Leyva, E. Moctezuma, M. López, K.M. Baines, B. Zermeño, Photocatalytic degradation of β-blockers in TiO_2 with metoprolol as model compound. Intermediates and total reaction mechanism, Catal. Today 323 (2019) 14–25.

[10] X. Yang, R. Zou, K. Tang, H.R. Andersen, I. Angelidaki, Y. Zhang, Degradation of metoprolol from wastewater in a bio-electro-Fenton system, Sci. Total Environ. 771 (2021), 145385.

[11] K.P. Gopinath, N.V. Madhav, A. Krishnan, R. Malolan, G. Rangarajan, Present applications of titanium dioxide for the photocatalytic removal of pollutants from water: a review, J. Environ. Manag. 270 (2020), 110906.

[12] J.G. Piedra López, O.H. González Pichardo, J.A. Pinedo Escobar, D.A. de Haro del Río, H. Inchaurregui Méndez, L.M. González Rodríguez, Photocatalytic degradation of metoprolol in aqueous medium using a TiO_2/natural zeolite composite, Fuel 284 (2021), 119030.

[13] Y. Ye, Y. Feng, H. Bruning, D. Yntema, H.H.M. Rijnaarts, Photocatalytic degradation of metoprolol by TiO_2 nanotube arrays and UV-LED: effects of catalyst properties, operational parameters, commonly present water constituents, and photo-induced reactive species, Appl. Catal. B: Environ. 220 (2018) 171–181.

[14] S. Sood, A. Umar, S.K. Mehta, S.K. Kansal, Highly effective Fe-doped TiO_2 nanoparticles photocatalysts for visible-light driven photocatalytic degradation of toxic organic compounds, J. Colloid Interface Sci. 450 (2015) 213–223.

[15] M.-C. Wu, P.-Y. Wu, T.-H. Lin, T.-F. Lin, Photocatalytic performance of Cu-doped TiO_2 nanofibers treated by the hydrothermal synthesis and air-thermal treatment, Appl. Surf. Sci. 430 (2018) 390–398.

[16] N. Serpone, Y.M. Artemev, V.K. Ryabchuk, A.V. Emeline, S. Horikoshi, Light-driven advanced oxidation processes in the disposal of emerging pharmaceutical contaminants in aqueous media: a brief review, Curr. Opin. Green Sustain. Chem. 6 (2017) 18–33.

[17] Y.-q Gao, J. Zhang, C. Li, F.-x Tian, N.-y Gao, Comparative evaluation of metoprolol degradation by UV/chlorine and UV/H_2O_2 processes, Chemosphere 243 (2020), 125325.

[18] A. Jaén-Gil, G. Buttiglieri, A. Benito, J.A. Mir-Tutusaus, R. Gonzalez-Olmos, G. Caminal, D. Barceló, M. Sarrà, S. Rodriguez-Mozaz, Combining biological processes with UV/H_2O_2 for metoprolol and metoprolol acid removal in hospital wastewater, Chem. Eng. J. 404 (2021), 126482.

[19] L. Hurtado, R. Romero, A. Mendoza, S. Brewer, K. Donkor, R.M. Gómez-Espinosa, R. Natividad, Paracetamol mineralization by Photo Fenton process catalyzed by a Cu/Fe-PILC under circumneutral pH conditions, J. Photochem. Photobiol. A: Chem. 373 (2019) 162–170.

[20] V. Romero, S. Acevedo, P. Marco, J. Giménez, S. Esplugas, Enhancement of Fenton and photo-Fenton processes at initial circumneutral pH for the degradation of the β-blocker metoprolol, Water Res. 88 (2016) 449–457.

[21] R.P. Cavalcante, R.F. Dantas, H. Wender, B. Bayarri, O. González, J. Giménez, S. Esplugas, A. Machulek, Photocatalytic treatment of metoprolol with B-doped TiO_2: effect of water matrix, toxicological evaluation and identification of intermediates, Appl. Catal. B: Environ. 176 (2015) 173–182.

[22] V. Romero, O. González, B. Bayarri, P. Marco, J. Giménez, S. Esplugas, Performance of different advanced oxidation technologies for the abatement of the beta-blocker metoprolol, Catal. Today 240 (2015) 86–92.

[23] F. Bensouici, M. Bououdina, A.A. Dakhel, R. Tala-Ighil, M. Tounane, A. Iratni, T. Souier, S. Liu, W. Cai, Optical, structural and photocatalysis properties of Cu-doped TiO_2 thin films, Appl. Surf. Sci. 395 (2017) 110–116.

[24] R. López, R. Gómez, M.E. Llanos, Photophysical and photocatalytic properties of nanosized copper-doped titania sol–gel catalysts, Catal. Today 148 (2009) 103–108.

[25] L.G. Devi, S.G. Kumar, B.N. Murthy, N. Kottam, Influence of Mn^{2+} and Mo^{6+} dopants on the phase transformations of TiO_2 lattice and its photo catalytic activity under solar illumination, Catal. Commun. 10 (2009) 794–798.

[26] X. Chen, S.S. Mao, Titanium dioxide nanomaterials: synthesis, properties, modifications, and applications, Chem. Rev. 107 (2007) 2891–2959.

[27] K.S.W. Sing, D.H. Everett, R.A.W. Haul, L. Moscou, R.A. Pierrot, J. Rouquerol, T. Siemieniewska, Reporting physisorption data for gas/solid systems with special reference to the determination of surface area and porosity, Pure Appl. Chem. 57 (1985) 603–619.

[28] M. Sahu, P. Biswas, Single-step processing of copper-doped titania nanomaterials in a flame aerosol reactor, Nanoscale Res. Lett. 6 (2011) 441.

[29] O. Avilés-García, J. Espino-Valencia, R. Romero, J.L. Rico-Cerda, R. Natividad, Oxidation of 4-chlorophenol by mesoporous titania: effect of surface morphological characteristics, Int. J. Photoenergy (2014), 210751.

[30] M. Crişan, M. Răileanu, N. Drăgan, D. Crişan, A. Ianculescu, I. Niţoi, P. Oancea, S. Şomăcescu, N. Stănică, B. Vasile, C. Stan, Sol–gel iron-doped TiO_2 nanopowders with photocatalytic activity, Appl. Catal. A: Gen. 504 (2015) 130–142.

[31] U. Diebold, The surface science of titanium dioxide, Surf. Sci. Rep. 48 (2003) 53–229.
[32] L. Samet, K. March, O. Stephan, N. Brun, F. Hosni, F. Bessousa, J. Benasseur, R. Chtourou, Radiocatalytic Cu-incorporated TiO_2 nano-particles for the degradation of organic species under gamma irradiation, J. Alloy. Compd. 743 (2018) 175–186.
[33] S. George, S. Pokhrel, Z. Ji, B.L. Henderson, T. Xia, L. Li, J.I. Zink, A.E. Nel, L. Mädler, Role of Fe doping in tuning the band gap of TiO_2 for the photo-oxidation-induced cytotoxicity paradigm, J. Am. Chem. Soc. 133 (2011) 11270–11278.
[34] K. Nagaveni, M.S. Hegde, G. Madras, Structure and photocatalytic activity of $Ti_{1-x}M_xO_{2\pm\delta}$ (M = W, V, Ce, Zr, Fe, and Cu) synthesized by solution combustion method, J. Phys. Chem. B 108 (2004) 20204–20212.
[35] X. Zhang, H. Tian, X. Wang, G. Xue, Z. Tian, J. Zhang, S. Yuan, T. Yu, Z. Zou, The role of oxygen vacancy-Ti^{3+} states on TiO_2 nanotubes' surface in dye-sensitized solar cells, Mater. Lett. 100 (2013) 51–53.
[36] A.S. Ethiraj, D.J. Kang, Synthesis and characterization of CuO nanowires by a simple wet chemical method, Nanoscale Res. Lett. 7 (2012) 70.
[37] J. Zhang, L.J. Xu, Z.Q. Zhu, Q.J. Liu, Synthesis and properties of (Yb, N)-TiO_2 photocatalyst for degradation of methylene blue (MB) under visible light irradiation, Mater. Res. Bull. 70 (2015) 358–364.
[38] M. Dorraj, M. Alizadeh, N.A. Sairi, W.J. Basirun, B.T. Goh, P.M. Woi, Y. Alias, Enhanced visible light photocatalytic activity of copper-doped titanium oxide–zinc oxide heterojunction for methyl orange degradation, Appl. Surf. Sci. 414 (2017) 251–261.
[39] B. Chen, A.J. Haring, J.A. Beach, M. Li, G.S. Doucette, A.J. Morris, R.B. Moore, S. Priya, Visible light induced photocatalytic activity of $Fe^{3+/}Ti^{3+}$ co-doped TiO_2 nanostructures, RSC Adv. 4 (2014) 18033–18037.
[40] D. Šojić, V. Despotović, D. Orčić, E. Szabó, E. Arany, S. Armaković, E. Illés, K. Gajda-Schrantz, A. Dombi, T. Alapi, E. Sajben-Nagy, A. Palágyi, Cs Vágvölgyi, L. Manczinger, L. Bjelica, B. Abramović, Degradation of thiamethoxam and metoprolol by UV, O_3 and UV/O_3 hybrid processes: kinetics, degradation intermediates and toxicity, J. Hydrol. 472–473 (2012) 314–327.
[41] J.G. Mahy, C. Wolfs, A. Mertes, C. Vreuls, S. Drot, S. Smeets, S. Dircks, A. Boergers, J. Tuerk, S.D. Lambert, Advanced photocatalytic oxidation processes for micropollutant elimination from municipal and industrial water, J. Environ. Manag. 250 (2019), 109561.
[42] F.J. Rivas, O. Gimeno, T. Borralho, M. Carbajo, UV-C radiation based methods for aqueous metoprolol elimination, J. Hazard. Mater. 179 (2010) 357–362.
[43] O. Alvarado-Rolón, A. Ramírez-Serrano, J. Ramírez-García, J. Orozco, R. Natividad, Kinetic modelling of Paracetamol degradation by photocatalysis: incorporating the competition for photons by the organicmolecule and the photocatalyst, J. Photochem. Photobiol. A: Chem. (2021).
[44] B. Abramović, S. Kler, D. Šojić, M. Laušević, T. Radović, D. Vione, Photocatalytic degradation of metoprolol tartrate in suspensions of two TiO_2-based photocatalysts with different surface area. Identification of intermediates and proposal of degradation pathways, J. Hazard. Mater. 198 (2011) 123–132.
[45] V. Romero, N. De la Cruz, R.F. Dantas, P. Marco, J. Giménez, S. Esplugas, Photocatalytic treatment of metoprolol and propranolol, Catal. Today 161 (2011) 115–120.
[46] R.P. Cavalcante, R.F. Dantas, B. Bayarri, O. González, J. Giménez, S. Esplugas, A. Machulek, Photocatalytic mechanism of metoprolol oxidation by photocatalysts TiO_2 and TiO_2 doped with 5% B: primary active species and intermediates, Appl. Catal. B: Environ. 194 (2016) 111–122.
[47] L.A. Pérez-Estrada, S. Malato, W. Gernjak, A. Agüera, E.M. Thurman, I. Ferrer, A. R. Fernández-Alba, Photo-Fenton degradation of diclofenac: identification of main intermediates and degradation pathway, Environ. Sci. Technol. 39 (2005) 8300–8306.
[48] V. Romero, P. Marco, J. Giménez, S. Esplugas, Adsorption and photocatalytic decomposition of the -blocker metoprolol in aqueous titanium dioxide suspensions: kinetics, intermediates, and degradation pathways, Int. J. Photoenergy 10 (2013).
[49] M.L. Wilde, W.M.M. Mahmoud, K. Kümmerer, A.F. Martins, Oxidation–coagulation of β-blockers by $K_2Fe^{VI}O_4$ in hospital wastewater: assessment of degradation products and biodegradability, Sci. Total Environ. 452 (2013) 137–147.
[50] V. Romero, F. Méndez-Arriaga, P. Marco, J. Giménez, S. Esplugas, Comparing the photocatalytic oxidation of Metoprolol in a solarbox and a solar pilot plant reactor, Chem. Eng. J. 254 (2014) 17–29.
[51] H. Yang, T. An, G. Li, W. Song, W.J. Cooper, H. Luo, X. Guo, Photocatalytic degradation kinetics and mechanism of environmental pharmaceuticals in aqueous suspension of TiO_2: a case of β-blockers, J. Hazard. Mater. 179 (2010) 834–839.
[52] V. Moradi, M.B.G. Jun, A. Blackburn, R.A. Herring, Significant improvement in visible light photocatalytic activity of Fe doped TiO_2 using an acid treatment process, Appl. Surf. Sci. 427 (2018) 791–799.
[53] E. Craciun, L. Predoana, I. Atkinson, I. Jitaru, E.M. Anghel, V. Bratan, C. Gifu, C. Anastasescu, A. Rusu, V. Raditoiu, E. Vasile, M. Anastasescu, I. Balint, M. Zaharescu, Fe^{3+}-doped TiO_2 nanopowders for photocatalytic mineralization of oxalic acid under solar light irradiation, J. Photochem. Photobiol. A: Chem. 356 (2018) 18–28.
[54] X.-j Yang, S. Wang, H.-m Sun, X.-b Wang, J.-s Lian, Preparation and photocatalytic performance of Cu-doped TiO_2 nanoparticles, Trans. Nonferrous Met. Soc. China 25 (2015) 504–509.
[55] R.D. Chekuri, S.R. Tirukkovalluri, One step synthesis and characterization of copper doped sulfated titania and its enhanced photocatalytic activity in visible light by degradation of methyl orange, Chin. J. Chem. Eng. 24 (2016) 475–483.
[56] C. Galindo, P. Jacques, A. Kalt, Photodegradation of the aminoazobenzene acid orange 52 by three advanced oxidation processes: UV/H_2O_2, UV/TiO_2 and VIS/TiO_2: comparative mechanistic and kinetic investigations, J. Photochem. Photobiol. A: Chem. 130 (2000) 35–47.
[57] V. Romero, O. González, B. Bayarri, P. Marco, J. Giménez, S. Esplugas, Degradation of Metoprolol by photo-Fenton: comparison of different photoreactors performance, Chem. Eng. J. 283 (2016) 639–648.
[58] E. Isarain-Chávez, J.A. Garrido, R.M. Rodríguez, F. Centellas, C. Arias, P.L. Cabot, E. Brillas, Mineralization of Metoprolol by electro-Fenton and photoelectro-Fenton processes, J. Phys. Chem. A 115 (2011) 1234–1242.
[59] B. Czech, P. Zygmunt, Z.C. Kadirova, K. Yubuta, M. Hojamberdiev, Effective photocatalytic removal of selected pharmaceuticals and personal care products by elsmoreite/tungsten oxide@ZnS photocatalyst, J. Environ. Manag. 270 (2020), 110870.